

## Zr-MOF-808@MCM-41 catalyzed phosgene-free synthesis of polyurethane precursors

Received 00th January 20xx,  
Accepted 00th January 20xx

DOI: 10.1039/x0xx00000x

www.rsc.org/

Sergio Rojas-Buzo,<sup>a</sup> Pilar García-García\*<sup>a</sup> and Avelino Corma\*<sup>a</sup>

In this work, a catalytic method is presented for the synthesis of aromatic carbamates from aromatic amines using dimethyl carbonate instead of phosgene as a green and safe reaction process. Microcrystalline Zr-MOF-808 is reported as an active and efficient heterogeneous catalyst for the selective carbamylation of anilines and industrially relevant aromatic diamines, under mild reaction conditions with near quantitative yields. We have accomplished the selective growth of well-dispersed Zr-MOF-808 nanocrystals within the mesoporous material MCM-41. A superior catalytic performance of the Zr-MOF-808@MCM-41 is demonstrated that together with increased stability stands out as an advantageous heterogeneous catalyst for polyurethane production. In situ FTIR studies have allowed a better understanding of the reaction pathway at the molecular level when the active MOF catalyst is present.

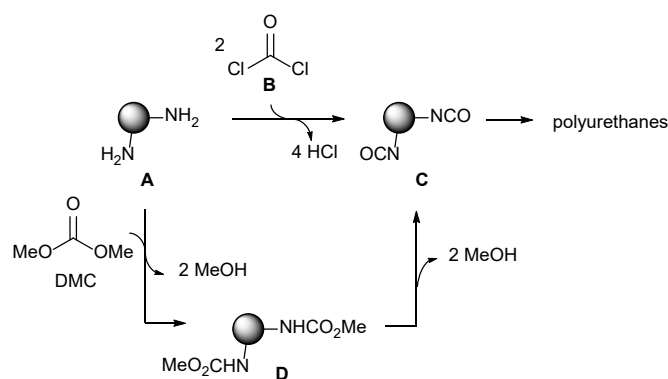
### Introduction

Aromatic polyurethanes are an important class of polymeric materials with a market size of 54 billion USD in 2015, which is anticipated to grow at a CAGR (compound annual growth rate) of more than 7% from 2016 to 2025. At present, the commercial method for synthesizing polyurethanes is based on the use of phosgene **B** (Scheme 1). Aromatic diisocyanates **C** are raw materials in the production of polyurethanes and they are prepared by the direct reaction of aromatic diamines **A** with phosgene **B** (Scheme 1). While the environmental and safety problems associated with phosgene have been recognized already several decades ago and have indeed triggered extensive research in the development of alternative chemical procedures precluding its usage, the reality is that phosgene-methods are still prevalent. New, cost effective and environmentally friendly synthetic procedures should be developed for the production of these commercially valuable intermediates.

In the case of aromatic diisocyanates **C**, the alternative synthetic strategy that appears more appealing consists in a two-step sequence wherein aromatic diamines **A** are transformed first to the dicarbamates **D** that after a thermal treatment give the desired diisocyanate products **C** (Scheme 1). In this regard, several methods have been reported for the synthesis of carbamates from amines. Among them, the

reaction with organic carbonates such as dimethyl carbonate, DMC, (Scheme 1) stands out as an excellent, safe, clean and green process with the generation of methanol as the only by-product in the transformation. The latter could be even further recycled in the production of dimethyl carbonate through a catalytic carbonylation reaction. Following this procedure, a zero-emission process can be realized, and this synthetic route has gained increasing interest.

Dimethyl carbonate (DMC) is considered a good example of a green compound due to its non-toxicity, good biodegradability and clean industrial methods of synthesis.<sup>1, 2</sup> On these bases, DMC appears as an excellent candidate to substitute phosgene in the bulk preparation of diisocyanates. However, there are several aspects that limit its application: 1) dimethylcarbonate exhibits low reactivity at moderate temperature and consequently it should be used in combination of a catalyst. 2) its dual behavior<sup>3</sup> as methylating and carbamoylating reagent can lead to low selectivity towards the desired *N*-carbamoylated derivative.



**Scheme 1.** Synthetic route to polyurethanes involving either phosgene or dimethyl carbonate.

<sup>a</sup> Instituto de Tecnología Química, UPV-CSIC, Universitat Politècnica de València-Consejo Superior de Investigaciones Científicas. Avenida de los Naranjos s/n 46022 Valencia, Spain. Email: pgargar@itq.upv.es; acorma@itq.upv.es

† Footnotes relating to the title and/or authors should appear here.

Electronic Supplementary Information (ESI) available: [details of any supplementary information available should be included here]. See DOI: 10.1039/x0xx00000x

Therefore, highly active and selective catalysts are needed to implement DMC as reagent in organic synthesis, and extensive research has been performed in this regard.

While aliphatic amines react smoothly with DMC to form the corresponding carbamates,<sup>4</sup> aromatic amines find struggle in this procedure owing to the inherent lower nucleophilicity. Several homogeneous and heterogeneous catalytic systems have been developed for the *N*-carbamoylation of aromatic amines with DMC. Homogeneous catalysts are lead compounds,<sup>5, 6</sup> zinc derivatives,<sup>7-15</sup> Yb(OTf)<sub>3</sub><sup>16</sup> and organocatalysts.<sup>17, 18</sup> Among these, Zn(OAc)<sub>2</sub> often gives the best activity for aromatic dicarbamate synthesis.<sup>7-9, 12, 13, 19</sup> However, it possesses certain drawbacks. Apart from the separation and recovery of the homogeneous catalyst, it was found that it loses activity easily because of its transformation to ZnO by reaction with methanol<sup>13</sup> which is the byproduct in the procedure. To overcome these problems, several studies have been performed dealing with immobilization of such catalyst into different supports. Zn(OAc)<sub>2</sub> supported on activated carbon allow carbamate formation from aniline and DMC in 78% yield, though extensive leaching is reported resulting in a loss of activity.<sup>20</sup> Zinc alkylcarboxylates have been covalently grafted in several types of silica materials such as SBA-15<sup>21</sup> and in plain SiO<sub>2</sub>.<sup>22</sup> Zn(OAc)<sub>2</sub>/SiO<sub>2</sub> material has been prepared by incipient impregnation and affords *N*-phenyl carbamate from aniline and DMC in 94% yield.<sup>23</sup> With these strategies, improved stability of Zn(OAc)<sub>2</sub> has been achieved and certain recyclability of the materials was probed. As an example, for the latter Zn(OAc)<sub>2</sub>/SiO<sub>2</sub> material, the authors report a drop in *N*-phenyl carbamate yield to 38% after the fifth use.<sup>23</sup> A polystyrene supported zinc complex have been recently shown to efficiently produce carbamates from anilines using DMC.<sup>24</sup> Several other heterogeneous catalysts have been found to promote the carbamoylation of aniline at different degrees of selectivity. Zirconia supported on SiO<sub>2</sub> affords *N*-phenyl carbamate from aniline and DMC in 80% yield (at 170°C during 7 hours).<sup>25</sup> Al-SBA-15 gives the same product with 71% selectivity after 3 hours reacting at 100°C.<sup>26</sup> ZnO-TiO<sub>2</sub> also allows formation of the same product from aniline in moderate yield of 67% (170°C, 7 hours).<sup>27</sup> Basic zinc carbonate has been used as a heterogenous catalyst in the same reaction yielding the desired carbamoylated product in 94% yield, and it could be further reused with a moderate decrease in the selectivity.<sup>10</sup> This latter system has also allowed to carry out the carbamoylation reaction of aniline in a fixed-bed continuously fed reactor.<sup>28</sup> A nanostarchfunctionalized ionic liquid containing a cobalt chelate anion have been successfully applied in the carbamoylation reaction of anilines and aliphatic amines by the reaction with DMC.<sup>29</sup> Curiously, all of the above heterogeneous catalysts have been exclusively tested in the carbamoylation reaction of aniline with DMC. While that transformation is extensively studied and optimized in terms of reaction temperature, catalyst loading and DMC to aniline ratio, the procedure was not extended to other substituted anilines and neither to the more challenging and also industrially relevant, aromatic diamines such as toluene diamines or 4,4'-methylene dianiline.

Probably the most active heterogeneous catalyst reported hitherto for the carbamoylation of aromatic diamines is based on gold-doped nanoparticulated-ceria.<sup>30, 31</sup> This is a highly effective and selective heterogeneous catalyst for the carbamoylation reaction of toluene diamine (and other anilines) that affords the product in 96% yield (140°C, 7 hours).<sup>30, 31</sup> Furthermore, the solid could be reused up to 3 times without apparent change in the activity. Due to the economic impact of these carbamate products, and the obvious advantages of phosgene-free synthetic routes, the search for new, better-performing and heterogeneous catalysts remains quite active.

Metal-organic frameworks (MOFs) are crystalline and three-dimensional reticular structures formed by organic ligands coordinatively bonded to metal ions or metal ion clusters.<sup>32-34</sup> The high metal concentration together with some other interesting properties such as modularity, high surface area and porosity, organic-inorganic hybrid composition, active-site uniformity and well-defined structures make these solid materials interesting candidates to address several challenges relating to energy and environmental suitability,<sup>35</sup> such as gas separation, hydrogen storage, carbon dioxide capture and heterogeneous catalysis.<sup>36-40</sup> To facilitate applications of MOFs to key market sectors such as industrial chemical synthesis, it is essential that the final solid catalyst displays further characteristics such as thermal, chemical and mechanical stability. In this regard, Zr-based MOFs feature exceptional stability (together with acid-base properties) which makes them especially attractive candidates in heterogeneous catalysis.<sup>41</sup> In addition, the versatility of Zr-based nodes as structural elements leads to a number of high porosity MOFs with diverse organic linkers, topologies and, potentially, with different catalytic activities. To date, Zr<sub>6</sub> MOFs with 12-, 10-, 8- and 6-connected nodes have been reported. We have here selected UiO-66 (Zr) MOF (12-connected) and Zr-MOF-808 (6-connected) for further investigations. Recent reports account for the higher catalytic activity observed for Zr-MOF-808 (6-connected) compared to UiO-66 (Zr) MOF (ideally 12-connected) in a variety of transformations such as the Brønsted acid catalyzed regioselective ring-opening reactions of epoxides,<sup>42</sup> hydrolysis of nerve-agent simulants<sup>43</sup> and catalytic transfer hydrogenation of carbonyls using alcohols as hydrogen donors.<sup>44, 45</sup> This activity difference is attributed to the coordinatively unsaturated units existing by design in Zr-MOF-808, together with the presence of larger apertures that facilitate delivery of the reacting starting materials to the interior of the MOF, thus enabling a much greater percentage of nodes to act as catalysts.

We here show that microcrystalline Zr-MOF-808 is an active and efficient heterogeneous catalyst for the highly selective carbamoylation reaction of anilines and industrially relevant aromatic diamines. Furthermore, we have accomplished the growth of the Zr-MOF in the mesoporous silica material MCM-41. In this manner, highly dispersed and nano-sized crystals of the MOF are attained and the resultant solid exhibits higher activity and stability in the aforementioned reaction.

## Results and discussion

Previous studies have described the utilization of various MOFs materials as heterogeneous catalysts in the reaction of aromatic amines with dimethylcarbonate.<sup>46</sup> It was reported that  $\text{Al}_2(\text{BDC})_3$  (BDC = 1,4-benzenedicarboxylate),  $\text{Fe}(\text{BTC})$  and  $\text{Cu}_3(\text{BTC})_2$  (BTC = 1,3,5-benzenetricarboxylate) promote methylation of aromatic amines in the reaction with DMC. Although there are some differences in the activity and selectivity, depending on the nature of MOFs, (poly)methylation is the predominant pathway.

For the present work, we have selected several Zr and Hf-based MOFs that have been prepared following recently reported procedures.<sup>42, 47</sup> UiO-66(Zr) and UiO-66(Hf) with the nominal chemical formula  $[\text{M}_6\text{O}_4(\text{OH})_4(\text{BDC})_{12}]$  were obtained using a solvothermal synthetic method by heating solutions containing  $\text{ZrCl}_4$  or  $\text{HfCl}_4$ , respectively, and terephthalic acid (1,4-benzenedicarboxylic acid,  $\text{BDCH}_2$ ) in dimethyl formamide employing formic acid as a modulating agent.<sup>47</sup> UiO-66- $\text{NH}_2$ (Hf) features the 2-aminoterephthalate as organic linker and was prepared using the same procedure except that 2-aminoterephthalic acid was used instead of terephthalic acid. In defect-free UiO-66 frameworks, a 12-coordination environment is presented in the  $\text{Zr}_6$  or  $\text{Hf}_6$  metal nodes.  $\text{Zr}_6$ -based MOFs with lower connectivity such as NU-1000 (8-connected) or MOF-808 (6-connected) have demonstrated superior catalytic activities in several reactions when compared to the UiO-66 (12-connected) materials.<sup>42-44</sup> We hypothesized that the coordinatively unsaturated centers in MOF-808 materials together with the larger apertures (calculated pore diameters of 4.8 and 18.4 Å versus 8 and 11 Å in UiO-66) could be beneficial for attaining selectivity in the catalytic carbamoylation reaction, whose transition state requires larger space than the competitive methylation reaction when DMC reacts with aromatic amines. Consequently, Zr-MOF-808 and Hf-MOF-808, with the nominal chemical formula  $[\text{M}_6\text{O}_4(\text{OH})_4(\text{BTC})_2(\text{HCOO})_6]$  were also prepared within this work by means of the corresponding solvothermal process using 1,3,5-benzenetricarboxylic acid ( $\text{BTCH}_3$ ) as the organic linker.<sup>42</sup> The MOF materials prepared within this work have been characterized (ESI) and the obtained data correlate well with those reported previously. However, in our hands, in the case of MOF-808 materials (Figure 1), we notice that the  $\text{N}_2$  sorption isotherms at 77K showed a mild hysteresis between adsorption and desorption branches (Figure 2a and Figure S16 in ESI) indicating

hierarchical micro/mesoporous textures. That fact was not reported previously for this type of solids,<sup>48</sup> although several reports account on this point in UiO-66 type materials.<sup>49</sup> Interestingly, the pore size distribution calculated using the Barrett-Joyner-Halenda (BJH) model suggests the existence of mesopores with a size of 3.8 nm for both Zr-MOF-808 and Hf-MOF-808 (Figure 2b and S17 in ESI, respectively). The pore size distribution in the microporous range could be estimated by the Ar adsorption isotherm (Figure S23, ESI) measured for Zr-MOF-808 and using the Hörvath-Kawazoe model that evidences a microporous size of 16.4 Å (Figure 2c), further demonstrating the hierarchical porosity of this material. Unfortunately, the smaller pore in the range of 4.8 Å calculated for Zr-MOF-808<sup>48</sup> could not be detected by using this particular technique. The observed hierarchical porosity of MOF-808 is shown here for the first time, as far as we know, and could be a result of missing linkers and clusters in the ideal MOF-808 framework. This unique feature could be beneficial for heterogeneous catalysis because of the dense catalytic sites packed in micropores and facile mass transfer through mesopores, as has been suggested in other MOF systems.<sup>50</sup>

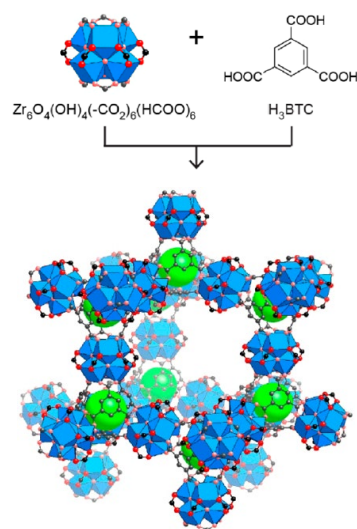


**Figure 1.** Zr-based secondary building units combined with 1,3,5-benzenetricarboxylic acid as organic linkers to form Zr-MOF-808. Atom color scheme: C, black or grey; O, red; Zr coordinated polyhedral, blue. Green spheres fill small tetrahedral cages. Figure reprinted with permission from Ref <sup>51</sup>. Copyright 2014 American Chemical Society.

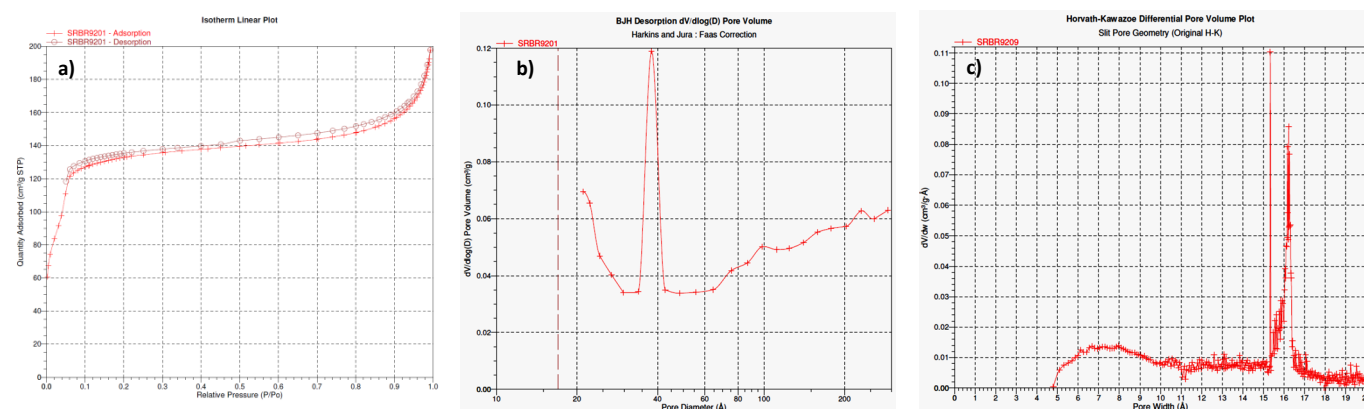


**Figure 2.** (a) N<sub>2</sub> adsorption (+) and desorption (o) isotherm of Zr-MOF-808 sample. (b) Pore size distribution of Zr-MOF-808 calculated by BJH model. (c) Pore size distribution of Zr-MOF-808 calculated by the Horvath-Kawazoe model.

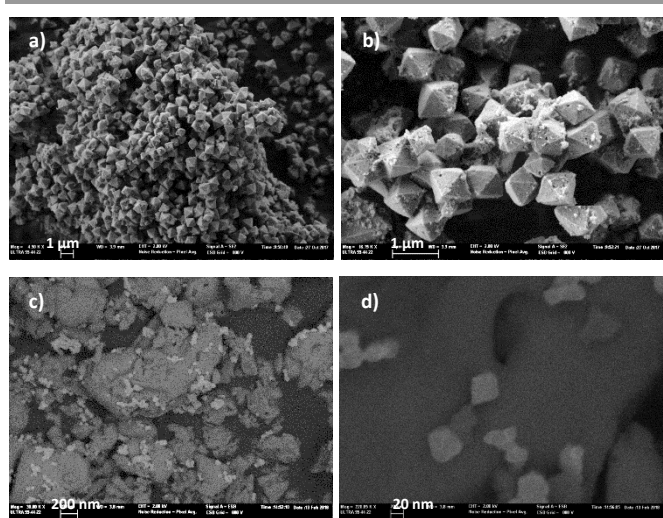


**Figure 3.** Field emission scanning electron microscopy (FESEM) images of (a) and (b) Hf-MOF-808 microcrystals. (c) and (d) Zr-MOF-808@MCM-41. Scale bars are included in each micrograph.

Octahedral crystals of Hf-MOF-808 with a size between 500 and 1200 nm were observed by field emission scanning electron microscopy (FESEM) as it is shown in Figure 3 (a and b).

The above prepared Zr- and Hf-based MOFs have been tested in the reaction of *o*-toluidine (as a model aromatic amine) with dimethylcarbonate as carbamoylating agent and solvent. Initial experiments (see ESI) allowed us to narrow down experimental conditions to carry out the transformation. The reaction was followed over time by using gas chromatography and dodecane as internal standard. Figure 4 shows the kinetic

results when the reaction was performed at 120°C and using 30 mol% loading (based on the metal) of the corresponding MOF catalyst with a 12:1 DMC:*o*-toluidine molar ratio. In this transformation, several products could be expected (Figure 4). The desired carbamoylation product **1** was obtained with different selectivity depending on the MOF catalyst employed. *N*-methyl-*o*-toluidine, *N,N*-dimethyl-*o*-toluidine and *N*-methyl-*N*-carbamate-*o*-toluidine were also formed in some cases as a consequence of the dual behavior of DMC. No other byproducts were detected by gas chromatography. Figure 4a showcases yield to the carbamate product **1**. It was found that all the MOF catalysts tested promote the reaction of *o*-toluidine and DMC, while varied selectivity was attained to the desired carbamate product **1** (Figure 4a). It can be seen that UiO-66 materials are not selective in the transformation giving similar amounts of methylated and carbamoylated products. No significant activity difference was observed when different node metal, Hf or Zr, was employed, and neither when employing UiO-66-NH<sub>2</sub>(Hf) with the 2-aminoterephthalate linker. Interestingly, the procedure was found highly selective when the catalyst employed was Zr-MOF-808 that affords the carbamate product **1** in 93% yield at full conversion of the starting material with only a minor amount of methylated products formed. This superior selectivity could be related to the lower connectivity in Zr<sub>6</sub> clusters that together with the larger apertures found in MOF-808 catalyst versus UiO would favor the carbamoylation transition state. The related Hf-MOF-808 showed slightly lower selectivity (85% for the carbamate product **1**). That could be explained by the higher Brønsted acidity<sup>42</sup> exhibited by the μ<sub>3</sub>-OH groups of Hf clusters in Hf-MOF-808 compared to those in Zr-MOF-808, which would lead to methylated products in higher percentage with the former.

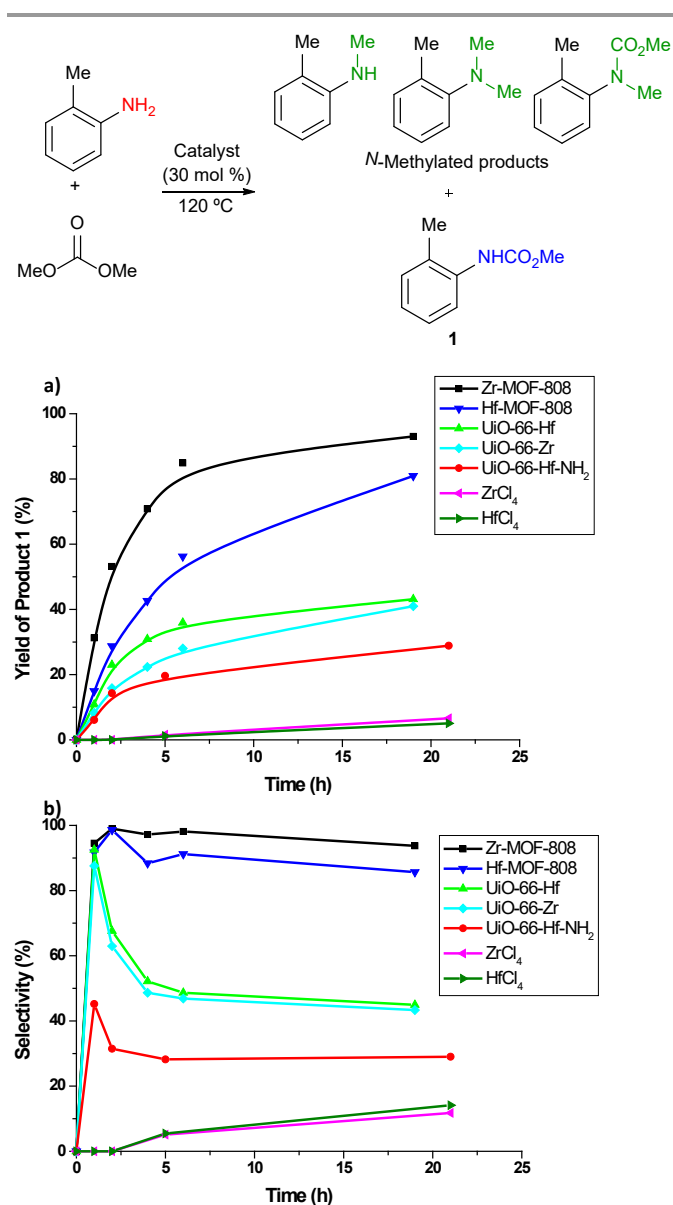


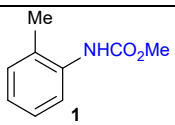
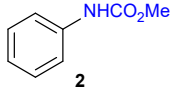
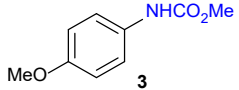
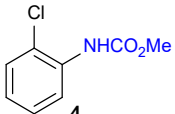
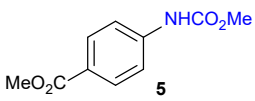
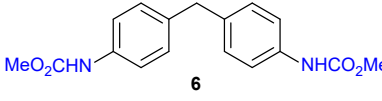
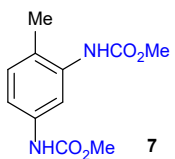
**Figure 4.** Hafnium and zirconium catalysts for the reaction of *o*-toluidine with DMC. Reaction conditions: 0.5 mmol *o*-toluidine, catalyst (30 mol% in metal), dodecane (35 mg) as internal standard, DMC (0.5 mL),  $T^{\text{a}}$  = 120 °C.

The reaction was also tested with the homogeneous catalysts ZrCl<sub>4</sub> and HfCl<sub>4</sub>, which showed a much lower activity and selectivity than the MOFs tested above due to the preferential formation of the methylated products with the former (Figure 4). The MOF component, 1,3,5-benzenetricarboxylic acid was also tested which resulted not active for the transformation (data not shown). The combination of ZrCl<sub>4</sub> and 1,3,5-benzenetricarboxylic acid as a catalytic system showed similar

behavior as ZrCl<sub>4</sub> on its own. Microcrystalline (5 μm, Sigma-Aldrich) and nanocrystalline (<100 nm, Sigma-Aldrich) ZrO<sub>2</sub> catalysts were also tested in the transformation (data not shown) and they were both found not active, yielding a small amount of methylated product along with unreacted starting material, under otherwise identical conditions. Hence, good results were attained with Zr-MOF-808 that was found an effective and selective catalyst for the carbamylation reaction of *o*-toluidine with DMC under mild reaction conditions.

The procedure was next extended to a variety of aromatic amines (Table 1). As an example, aniline can be efficiently converted to produce methyl phenylcarbamate **2** that was isolated in high yield of 92% (Table 1, entry 2). The presence of different substituents in the aromatic ring was also studied. For example, electron-donating groups such as *o*-methyl or *p*-methoxy didn't affect the efficiency in the transformation, and the carbamate product was isolated in 93 and 92%, respectively (Table 1, entries 1 and 3). The presence of electron withdrawing groups such as chloride (Table 1, entry 4) or an ester group (Table 1, entry 5) required longer reaction time, but the carbamate products were also formed with high selectivity. The procedure was also tested with industrially relevant aromatic diamines such as 4,4'-diaminodiphenylmethane (Table 1, entry 6) and 2,4-diaminotoluene (Table 1, entry 7). Dicarbamates **6** and **7** are direct precursors of aromatic diisocyanates, which in turn, are used in the bulk production of several polyurethane materials. Both products **6** and **7** are obtained here in good isolated yield with high selectivity, although higher reaction temperature was required to allow an efficient transformation with 20 mol% catalyst load. It should be noted that dicarbamate **6** could also be obtained by reaction of carbamate **2** with formaldehyde in the presence of an acidic catalyst such as zeolite H $\beta$ .<sup>52</sup> The kinetic profiles for the reaction of 2,4-diaminotoluene with DMC could be found in the ESI when using different catalyst loading. It was observed that at 120 °C with 30 mol% catalyst, only the *para*-carbamate product was mainly formed. When the temperature was raised to 150 °C, dicarbamate product **7** was obtained and a catalyst loading of 20 mol% was appropriate to afford the product in 91% yield after 10 hours reaction time.

**Table 1.** Carbamoylation reaction of several aromatic amines with DMC in the presence of Zr-MOF-808 and Zr-MOF-808@MCM-41.

| Entry | Carbamate   | Catalyst                                  |          |           |                          |  |          |                          |
|-------|---|---|----------|-----------|--------------------------|--|----------|--------------------------|
|       |   | Zr-MOF-808 <sup>[a]</sup> (20 or 30 mol%) |          |           |                          | Zr-MOF-808@MCM-41 <sup>[b]</sup> (2.5 or 5.0 mol%) |          |                          |
|       |   | T <sup>a</sup> (°C)                       | Time (h) | Conv. (%) | Yield <sup>[c]</sup> (%) | T <sup>a</sup> (°C)                                | Time (h) | Yield <sup>[c]</sup> (%) |
| 1     |    | 120                                       | 20       | 98        | 93                       | 160  | 3        | 85                       |
| 2     |    | 120                                       | 16       | 99        | 92                       | 160  | 2        | 89                       |
| 3     |  | 120                                       | 17       | 98        | 92                       | 160  | 2.5      | 90                       |
| 4     |  | 120                                       | 24       | 98        | 90                       | 160  | 5.2      | 84                       |
| 5     |  | 120                                       | 48       | 90        | 80                       | 160  | 5        | 89                       |
| 6     |  | 150                                       | 19       | 90        | 88 <sup>[d]</sup>        | 160  | 3        | 95 <sup>[e]</sup>        |
| 7     |  | 150                                       | 10       | 99        | 91 <sup>[d]</sup>        | 160  | 3        | 93 <sup>[e]</sup>        |

<sup>[a]</sup>Reaction conditions for catalyst Zr-MOF-808: 0.5 mmol of amine, Zr-MOF-808 (30 mol% in Zr), DMC (0.5 mL). <sup>[b]</sup>Reaction conditions for catalyst Zr-MOF-808@MCM-41: 0.5 mmol of amine, Zr-MOF-808@MCM-41 (2.5 mol% in Zr), DMC (0.5 mL). <sup>[c]</sup>Isolated yield after column chromatography. <sup>[d]</sup>Zr-MOF-808 (20 mol% in metal) was used, DMC (1 mL). <sup>[e]</sup>Zr-MOF-808@MCM-41 (5 mol% in Zr) was used.

We have also examined the heterogeneity and recyclability of Zr-MOF-808. A hot filtration test of the solid catalyst was performed after 1 hour reacting at 120°C which completely shuts down the reaction. The results indicate that no active species were leached to the reaction media from the solid catalyst and that Zr-MOF-808 acts as a true heterogeneous catalyst (Figure 5). Stability of the catalyst in the

carbamoylation reaction was next evaluated. With this intention, the catalyst was recovered after the reaction of *o*-toluidine was completed. It was then washed (with EtOAc) and dried before it was submitted to a second reaction cycle with a fresh solution. It was found that activity of the solid catalyst decreases significantly and the yield of the carbamate product **1** drops to 14% in the second run (Figure 5b). Analysis of the

powder XRD pattern of Zr-MOF-808 after utilization shows that crystallinity of the material is almost completely lost (Figure S33, ESI), which could explain the strong decrease of activity. The low stability of the material under the reaction conditions could explain the requirement of the relatively high catalyst loading (30 mol%) to achieve good conversion to the desired carbamate product.

In view of the poor stability of the catalyst Zr-MOF-808 under the reaction conditions, a new direction was explored. We considered the increasing awareness, that the typical MOF microcrystals obtained directly from the traditional solvothermal process are not necessarily the best configuration for the final application. Hence, the latest trends focus on the design of sophisticated hybrid materials based on MOFs as active functional species. Thus, MOFs are combined with different supports in order to integrate the physicochemical characteristics of both materials while avoiding their weaknesses as single components such as mechanical, thermal and chemical stability. Moreover, it could be expected that the support can add supplementary synergistic properties that might arise from the interactions in the resulting composite material. To this respect, MOFs confinement in porous materials has been demonstrated as an efficient strategy to enhance the dispersion and stability of MOFs,<sup>53, 54</sup> and mesoporous silica and zeolites appeared as ideal hosts due to their well-defined channels, large porosity and good thermal/chemical stability. We have carried out here the selective growth of MOF nanocrystals within mesoporous pure silica material MCM-41 (see ESI for experimental details). To achieve that, both precursor solutions (ZrCl<sub>4</sub> and ligand salt) were sequentially incorporated within pure silica MCM-41 via incipient wetness impregnation, including an intermediate step for the acidification of the organic ligand salt to the acid form via the gas phase (using hydrogen chloride). Each step is followed by a heating treatment at 50°C under vacuum to evacuate the water from the previous impregnation step. After that, the resulting dry solid was exposed to the specific MOF synthesis conditions in the presence of dimethyl formamide and formic acid. Finally, the product was washed with distilled water, dimethyl formamide and acetone.

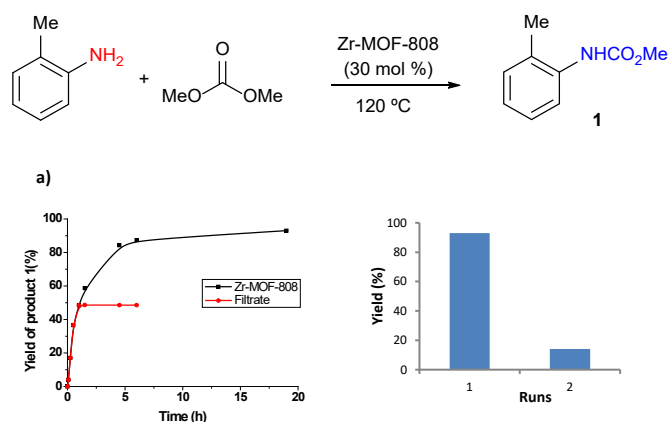


**Figure 5.**(a) Time-yield plots for the *N*-carbamoylation of *o*-toluidine with Zr-MOF-808 (black line) and removing the catalyst after 1 h (red line), and (b) catalyst reusability.

Reaction conditions: 0.5 mmol amine, catalyst (30 mol %), dodecane (35 mg) as internal standard, DMC (0.5 mL), T = 120 °C.

With this approach, two key advantages have been achieved for the implementation of Zr-MOF-808 as heterogeneous catalyst in the carbamoylation reaction of industrially relevant aromatic diamines, as will be shown below. In the first place, the concentration of catalytic active sites at the external crystal surface is maximized by reducing the crystals size down to the nanometer domain by confinement within the mesoporous platform. Secondly, the host protects and confers additional stability to the highly active catalytic MOF.

The Zr-MOF-808@MCM-41 here prepared was characterized and the XRD pattern shows the peaks corresponding to a typical MCM-41 material (Figure S25, ESI). It is observed one intense peak of (100) and two weak diffraction peaks of (110) and (200) indicating that the mesopore hexagonal order of the material was preserved after MOF crystallization. However, diffraction peaks corresponding to Zr-MOF-808 were not observed. It should be notice that diffraction peaks of Zr-MOF-808 are indeed observed when a physical mixture is prepared containing the two solids, i. e., the plain MCM-41 silica and microcrystalline Zr-MOF-808 (prepared separately by the traditional solvothermal process) with analogous Zr weight% than that measured in Zr-MOF-808@MCM-41 (3.2 Zrwt%). This phenomenon could be attributed to the small crystal size in Zr-MOF-808@MCM-41 that together with the high dispersion exceeds the detection limit of the XRD apparatus. Field emission scanning electron microscopy (FESEM) images show the presence of the two phases in Zr-MOF-808@MCM-41 (Figure 3, c and d). MOF crystals with a size around 20-40 nm are observed in the outer surface of the silica material. Elemental mapping evidences the zirconium content of the crystals observed. Other characterization techniques were used to provide evidence on the formation of the MOF on the mesoporous material. On the one hand, the UV/Vis spectra of Zr-MOF-808@MCM-41 show a main peak around 242 nm, which is attributed to the absorption of Zr-O clusters in this MOF, while the related band in, for instance, ZrO<sub>2</sub>nanopowder appeared at 229 nm (Figure S26, ESI) and those of ZrCl<sub>4</sub> are also observed at lower wavelengths. On the other hand, the FTIR spectra of Zr-MOF-808@MCM-41 shows several characteristic bands of Zr-MOF-808 such as those at 1380 and 1450 cm<sup>-1</sup> and also bands at 1580, 1663 and 1693 cm<sup>-1</sup> (Figure 7). Additionally, FTIR showed the disappearance of key vibrational band corresponding to carbonyl stretching vibration  $\nu(\text{C}=\text{O})$  of the carboxylic acid at 1720 cm<sup>-1</sup>, which confirmed the formation of the corresponding MOF.

The specific surface area of the resultant material was measured by N<sub>2</sub>physisorption experiment (Figure S28, ESI). As expected, it was observed a decrement in N<sub>2</sub> adsorption capacity and pore size for Zr-MOF-808@MCM-41 compared to the starting solid MCM-41. Unfortunately, Ar physisorption experiment did not reveal micropores around 16.4 Å corresponding to the Zr-MOF-808. We believe that the low MOF loading in the silica material (3.2 Zrwt% as determined by

ICP analysis) does not allow the pore size distribution estimation using the Hörvath-Kawazoe model. The  $^{13}\text{C}$  CP/MAS NMR spectrum of Zr-MOF-808@MCM-41 (Figure S29, ESI) shows the peaks corresponding to the organic linker, 1,3,5-benzenetricarboxylate and all the carbon atoms were unequivocally assigned and the signals appeared at the same ppm as in Zr-MOF-808 (broad band at 132-135 ppm corresponding to aromatic carbons and the peak at 169 ppm corresponding to the carboxylate carbon). Further confirmation of MOF formation is attained by the observation that the peak at 130 ppm corresponding to the  $C_{\text{ipso}}$  in 1,3,5-benzenetricarboxylic acid is not observed for Zr-MOF-808 and neither for Zr-MOF-808@MCM-41 for which the  $C_{\text{ipso}}$  of 1,3,5-benzenetricarboxylate falls in the peak at 132-135 ppm. The corresponding peak of formate ligand at 167 ppm was also detected for Zr-MOF-808@MCM-41 (Figure S29, ESI). XPS experiment additionally reveals MOF formation in the host with Zr (3d) bands at 180.8 and 182.9 for Zr-MOF-808 that appeared similarly in Zr-MOF-808@MCM-41 (Figures S30 and S31, ESI).

Finally, the obtained Zr-MOF-808@MCM-41 material was employed as catalyst for the carbamoylation reaction of aromatic diamines such as 2,4-diaminetoluene (Figure 7). Remarkably, a low catalyst loading (5 mol%) was enough to promote efficiently the transformation to the desired dicarbamoylated product **7**. Figure 7a shows the kinetic profile of the transformation wherein the highest yield of 88% of dicarbamate **7** was achieved after 2.5 hours reacting at 160°C, as determined by GC using dodecane as internal standard. Reported catalysts for this same transformation of 2,4-diaminetoluene to dicarbamate **7** are  $\text{Zn}(\text{OAc})_2 \cdot 2\text{H}_2\text{O}$ <sup>8</sup> and gold-doped nanoparticulated-ceria<sup>30</sup> that give the desired product **7** in 98 and 96% yield, respectively. While those both exhibit slightly higher selectivity than Zr-MOF-808@MCM-41 (93% isolated yield, see entry 7 in Table 1), the heterogeneous character of the material here reported offers additional advantages versus homogeneous catalyst  $\text{Zn}(\text{OAc})_2 \cdot 2\text{H}_2\text{O}$ . When comparing to gold-doped ceria,<sup>30</sup> the solid presented herein offers an alternative non-precious metal based solid catalyst with very high selectivity in the transformation.

For comparative purposes,  $\text{ZrO}_2$  nanopowder (< 100 nm, Sigma-Aldrich) was tested in the transformation and no activity was register even after extended time of 8 hours (ESI). The solid support, pure silica MCM-41, was also assayed in the same reaction and it was shown that it basically promotes (poly)methylation reaction although at a slower pace (ESI), in the sense that when Zr-MOF is present the high activity of the MOF precludes extensive methylation reaction. Comparison was also performed with a traditional  $\text{ZrO}_2$ @MCM-41 material that was obtained following a reported procedure<sup>55</sup> by wet impregnation of MCM-41 with  $\text{ZrOCl}_2 \cdot 8\text{H}_2\text{O}$  and subsequent calcination in air at 500°C for 2 hours. It was observed that the presence of  $\text{ZrO}_2$  nanocrystals in the MCM-41 matrix further accelerates the methylation reaction and the *para*-carbamate

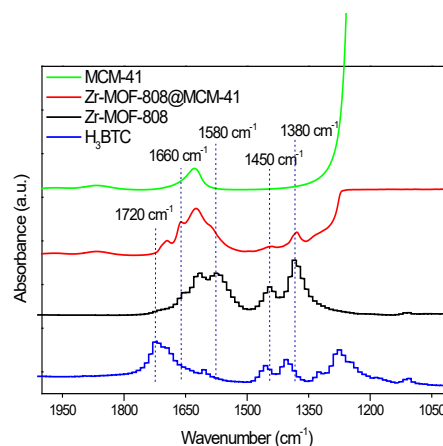


Figure 6. FTIR spectra

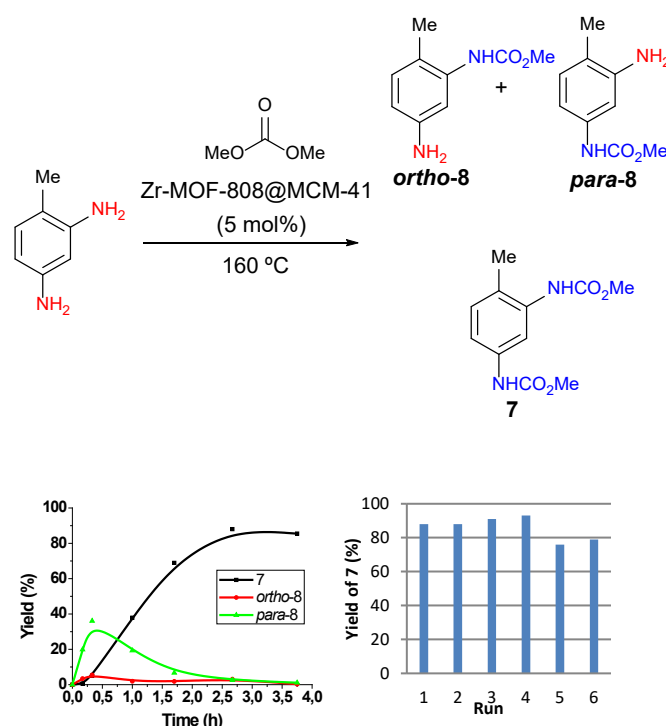


Figure 7. (a) Time-yield plots for the *N*-carbamoylation of 2,4-diaminetoluene with Zr-MOF-808@MCM-41. (b) catalyst reusability. Reaction conditions: 0.5 mmol amine, catalyst (5mol %), dodecane (35 mg) as internal standard, DMC (0.5 mL),  $T = 160\text{ }^\circ\text{C}$ .

product **8** was also detected although in low yield of 5% and after extended time of 8 hours with nearly completed conversion of the starting material (ESI). In the case of [Zr]MCM-41 in which the metal ions are incorporated in the framework replacing some silicon atoms, it has been reported previously that *N*-carbamoylated products are formed along with methylated products in similar ratio and therefore no selectivity was achieved in the transformation.<sup>56</sup> The heterogeneity and stability of Zr-MOF-808@MCM-41 was next evaluated. The hot filtration test showed the heterogeneous character of the catalyst employed (Figure S34, ESI). More importantly, the catalyst could be recovered and reused at least four times without apparent change in the



reaction efficiency and even slightly higher yields were attained in the subsequent three runs (Figure 7b). A slight activity decrease was observed from run number five. That was attributed to deposition of organic components in the solid that may block accessibility to the MOF active sites, since characterization of the reutilized material exhibited a substantial decrease in the BET surface area (from 777 m<sup>2</sup>g<sup>-1</sup> in as-synthesized Zr-MOF-808@MCM-41 to 464 m<sup>2</sup>g<sup>-1</sup> in the reutilized material) together with a higher organic content as determined by elemental analysis. However, XRD pattern showed similar to the starting material which entails supports stability under the reaction conditions by the preservation of the mesopores ordering.

We have carried out an in situ FTIR spectroscopy study to gain insight of what is occurring at the molecular level on the surface of the catalytically active MOF crystals. This spectroscopic investigation takes advantage of the fact that DMC and aniline (as a model aromatic amine) are both liquids, and they can be easily dosed from the gas phase onto the MCM-41 materials that, upon diffusion inside the pores, the IR spectrum of the wafer containing DMC and DMC+aniline can be easily recorded in situ. The available frequency range for the IR study on these MCM-41 materials (1900-1200 cm<sup>-1</sup>) only allows observation of the  $\nu(\text{CO})$  mode and the  $\nu_{\text{asymm.}}(\text{CO}_2)$  of the carbonyl bond in DMC (1810-1680 cm<sup>-1</sup> and 1320-1235 cm<sup>-1</sup>, respectively) and the  $\delta(\text{CH}_3)$  modes of the methyl groups (1400-1500 cm<sup>-1</sup>). The bands associated with,  $\nu_{\text{symm.}}(\text{CO}_2)$ ,  $\nu_{\text{symm.}}(\text{O-CH}_3)$ , and  $\nu_{\text{asymm.}}(\text{O-CH}_3)$ , which would be of high diagnostic utility, cannot be observed because they fall within the framework region.

In the first place, we have evaluated interaction of DMC with the active sites in the solid materials with the aim to determine structural perturbations induced in DMC upon interaction and, therefore, elucidate activation pathways that would account for the attained selectivity.

Figure 8 shows the FTIR spectra of bare DMC (Figure 8a), DMC adsorbed on MCM-41 solid (Figure 8b) and DMC adsorbed on Zr-MOF-808 (Figure 8c). Difference FTIR spectrum is shown in the latter case due to the framework signals that otherwise preclude observation of the vibrational modes assigned to DMC when adsorbed to this material. From the observation of these FTIR spectra we can infer that the interaction of DMC with these solids MCM-41 and Zr-MOF-808 induces a relevant perturbation of the molecule which influences the vibrational properties and hence, the force constants of bonds within the molecule. It will be shown that such interaction of DMC with the Zr sites in the MOF would explain why Zr-MOF-808 is so

effective in promoting the carboxymethylation activity of DMC.

DMC possesses two distinct nucleophilic sites as has been determined by analysis of the molecular electrostatic potential.<sup>57</sup> One nucleophilic site is located on the oxygen of the carbonyl group and the second one corresponds to the oxygen atoms of the O-C-O moiety. On this bases three different DMC adducts (Figure 9) could be formed when interacting with the zirconium sites (or with silanol groups in the case of MCM-41).

This approach has been demonstrated to be able to describe the electrostatic interaction between DMC molecule and Na<sup>+</sup> ions in the supercages of NaY zeolite.<sup>57</sup> In that study, it was concluded that when the interaction occurs through the oxygen in the carbonyl moiety (related structures I and II in Figure 9), the calculations predict an elongation (and therefore weakening) of the O-CH<sub>3</sub> bonds, a fact which would lead to the methylation reaction. While in adduct of type III, calculations predict an elongation/weakening of the C-OCH<sub>3</sub> bond, a fact that would facilitate delivery of the carbonylmethoxy group which hence justifies the catalytic activity in the carbamoylation reaction. The theoretical calculations performed in the case of NaY zeolite where complemented with experimental results studying the modification of the IR properties of DMC induced by the interaction with the zeolite.<sup>57</sup> It was concluded that for adducts I and II, the  $\nu(\text{CO})$  and  $\nu_{\text{asymm.}}(\text{CO}_2)$  are red- and blue-shifted, respectively, with respect to isolated DMC. Indeed, that fact was observed here in our case with MCM-41 (Figures 8a and 8b) wherein  $\nu(\text{CO})$  shifts from 1780 and 1768 cm<sup>-1</sup> (Figure 8a) to 1753, 1727 and 1688 cm<sup>-1</sup> (Figure 8b) when interacting with the MCM-41 surface. Additionally, a blue-shift from 1294 cm<sup>-1</sup> to 1310 cm<sup>-1</sup> is observed for the  $\nu_{\text{asymm.}}(\text{CO}_2)$  of DMC. The analogy could be established with the NaY zeolite study, and we could conclude that DMC interacts with the silanol groups in the surface of MCM-41 *via* structures of type I and II that are suggested to lead to methylation reaction, which was indeed, the observed experimental results obtained in the case of plain

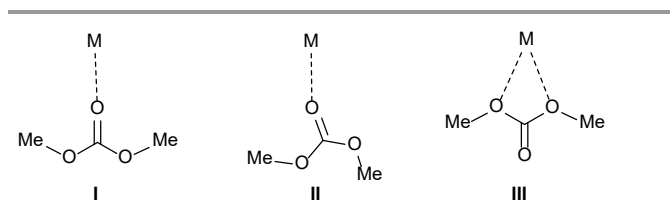
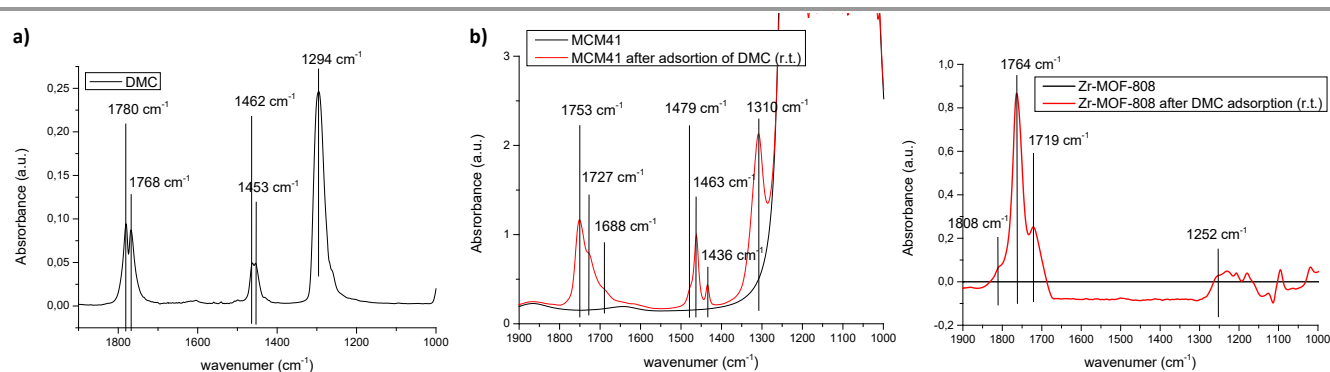


Figure 9. Possible DMC adducts formed upon interaction with the solid catalyst



**Figure 8.** (a) FTIR spectrum of bare DMC, (b) FTIR spectra of MCM-41 and MCM-41 after adsorption of DMC and (c) Difference FTIR spectra of Zr-MOF-808 and Zr-MOF-808 after adsorption of DMC.

siliceous material MCM-41. On the other hand, the IR properties of adduct **III** in zeolite NaY display an opposite behavior, with the  $\nu(\text{CO})$  blue-shifting and  $\nu_{\text{asymm.}}(\text{CO}_2)$  red-shifting with respect to isolated DMC. In the case of Zr-MOF-808, it was observed a blue-shift of  $\nu(\text{CO})$  from 1780 and 1768  $\text{cm}^{-1}$  (Figure 8a) to 1808  $\text{cm}^{-1}$  (Figure 8c) and a red-shift of  $\nu_{\text{asymm.}}(\text{CO}_2)$  from 1294  $\text{cm}^{-1}$  to 1252  $\text{cm}^{-1}$ . These data therefore suggest the presence of type **III** adducts upon interaction of DMC with the Lewis acidic sites in the MOF material in analogy to those results observed for DMC and NaY zeolite.<sup>57</sup> The presence of adducts **III** when using Zr-MOF-808 would account for the observed carbamoylation reaction attained by this catalyst due to the weakening of the C-OCH<sub>3</sub> bonds. Adducts of type **I** and **II** can not be ruled out for Zr-MOF-808 since a red-shift of  $\nu(\text{CO})$  to 1719  $\text{cm}^{-1}$  was also detected for this material (Figure 8c). Hence, it seems reasonable to conclude that the three adduct structures (Figure 9) could be present in the MOF case upon interaction of DMC with the active sites. Being type **III** structures the less stable,<sup>57</sup> that would react at higher rate than **I** and **II** allowing the carbamoylation reaction as the predominant pathway.

Further FTIR experiments were conducted. The results given in Figure 10a show the signals corresponding to DMC (around 1700-1800  $\text{cm}^{-1}$  and 1400-1500  $\text{cm}^{-1}$ ) upon adsorption on MCM-41. It is observed that upon desorption by applying vacuum both groups of signals experiment a decrease in their intensity to the same extent, and DMC is completely desorbed when further heated at 60°C. On the contrary, Zr-MOF-808@MCM-41 (Figure 10b) shows different intensity in both group of signals upon DMC desorption already at room temperature. A substantial decrease of the signal at 1750  $\text{cm}^{-1}$  (corresponding to the carbonyl group in DMC) is observed while those signals at 1490, 1460 and 1433  $\text{cm}^{-1}$  (corresponding to the methyl group in DMC) are still prevalent,

which would indicate an easier desorption (and potentially higher reactivity) of the carbonate than the methyl species when the MOF crystals are present in the MCM-41 matrix. Furthermore, in this case, the signals corresponding to the methyl group are still observed upon heating to 60°C while that of the carbonyl group (at 1750  $\text{cm}^{-1}$ ) has completely disappeared.

In a different set of experiments, aniline (1606  $\text{cm}^{-1}$ ) was introduced into the IR cell and subsequently DMC was co-adsorbed and the wafer was then heated at 60°C and 120°C (Figures 10c and 10d). No apparent change was observed by FTIR when co-adsorbing aniline and DMC on MCM-41 and heating the sample up to 120°C, at least in the timeframe used for the FTIR experiment (Figure 10c), which reveals the poor activity of the host. In the case of Zr-MOF-808@MCM-41 (Figure 10d), after co-adsorption of aniline and DMC and heating up to 60°C, a substantial decrease in the band at 1750  $\text{cm}^{-1}$  is already observed (while prevalence of the methyl bands around 1400-1500  $\text{cm}^{-1}$ ) which completely disappears at 120°C (that was not the case with plain MCM-41 in Figure 10c). Meanwhile, on Zr-MOF-808@MCM-41 it is observed an increment in the band at 1662  $\text{cm}^{-1}$ , which can be attributed to the carbonyl group of the newly formed carbamate product. Further increment of the latter band is observed when heating at 120°C which would indicate further product formation at that temperature. Taken together these results, they nicely explain the high efficacy of MOF-doped mesoporous silica in promoting the carbamoylation reaction and the preference of that product formation versus methylation when using DMC and aromatic amines.

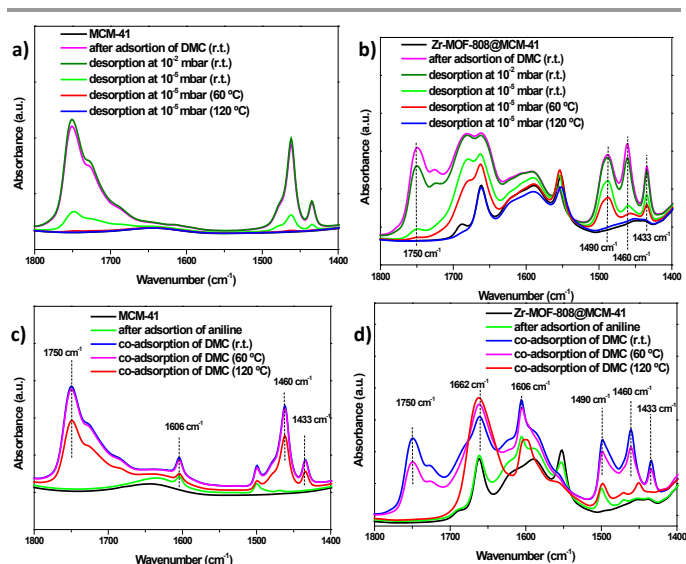


**Figure 10.** (a) FTIR spectra of MCM-41 before and after adsorption of DMC at room temperature, and subsequent DMC desorption at increasing temperatures (60 and 120°C). (b) FTIR spectra of Zr-MOF-808@MCM-41 before and after adsorption of DMC at room temperature, and subsequent DMC desorption at increasing temperatures (60 and 120°C). (c) FTIR spectra of MCM-41 before and after adsorption of aniline and co-adsorption of DMC at room temperature, and subsequent temperature raise (60 and 120°C). (d) FTIR spectra of Zr-MOF-808@MCM-41 before and after adsorption of aniline and co-adsorption of DMC at room temperature, and subsequent temperature raise (60 and 120°C).

Since Zr-MOF-808@MCM-41 exhibited remarkable activity in the carbamylation reaction of 2,4-diaminotoluene using DMC and additionally, high stability of the catalyst was probed by continuous reutilization, the method was extended to a variety of aromatic amines (Table 1). Analogously, 4,4'-diaminodiphenylmethane gave dicarbamate<sup>6</sup> in excellent yield of 95% (Table 1, entry 6). Several aromatic monoamines were also transformed efficiently to the monocarbamates. In these cases, a low loading of 2.5 mol% was sufficient to achieve high conversion of the carbamate products. The observed reactivity trend was similar as that one attained with microcrystalline Zr-MOF-808 and the presence of electro-withdrawing groups in the aromatic ring required extended reaction time (Table 1, entries 4 and 5) to achieve full conversion as compared to aromatic amines with electron-donating groups (Table 1, entries 1 and 3). In any case, the carbamate products were obtained with high yields and high selectivities. An aliphatic amine such as butylamine was found to react smoothly with DMC to form the corresponding carbamate at 100°C. The presence of the hybrid catalyst, in this particular case of aliphatic amine, did not provide additional rate or selectivity enhancement. On another matters, since the final goal is the large-scale application of this hybrid catalyst, a regular silica was also utilized for the preparation of the hybrid material Zr-MOF-808@SiO<sub>2</sub> following the same procedure as for MCM-41. In this way, comparable catalytic activity was measured for Zr-MOF-808@SiO<sub>2</sub> (1.9 wt%Zr) compared to Zr-MOF-808@MCM-41 (3.2 wt% Zr) (see ESI). While this study mainly focuses on MCM-41 host, these results further evidence the possibility of

using alternative silica materials for the preparation of related catalytically active hybrid MOF materials.

## Conclusions

We have shown that Zr-MOF-808 is an active and highly selective catalyst for the reaction of aromatic diamines with DMC to produce dicarbamate products required for the synthesis of aromatic polyurethanes. Furthermore, we have demonstrated the superior catalytic performance of the Zr-MOF-808@MCM-41 and Zr-MOF-808@SiO<sub>2</sub> with respect to the bulk microcrystalline Zr-MOF-808 solid. The increased catalytic activity and mechanical stability of this material allows for multiple reuses of the catalyst without significant leaching of the active sites. This process opens a route for polyurethane production that avoids the use of phosgene through the reactant DMC without generating any by-product except recyclable methanol. In situ FTIR studies allow a better understanding of the reaction pathway at the molecular level when the highly active MOF catalyst is present. Furthermore, the solid materials herein developed, Zr-MOF-808@MCM-41 and Zr-MOF-808@SiO<sub>2</sub> are potential highly active and stable catalyst for several other organic transformations wherein microcrystalline Zr-MOF-808 has proved successful, further expanding the scope and possibilities of the solids herein reported.

## Conflicts of interest

There are no conflicts to declare.

## Acknowledgements

This work was funded by the European Union through the European Research Council (grant ERC-AdG-2014-671093, SynCatMatch) and by the Spanish government through the Severo Ochoa program (SEV-2016-0683). S. R-B acknowledges a PhD fellowship from the Generalitat Valenciana. The Electron Microscopy Service of the Universitat Politècnica de València is acknowledged for their help in sample characterization.

## Notes and references

1. P. Tundo and M. Selva, *Acc. Chem. Res.*, 2002, **35**, 706-716.
2. G. Fiorani, A. Perosa and M. Selva, *Green Chem.*, 2018, **20**, 288-322.
3. P. Tundo, L. Rossi and A. Loris, *J. Org. Chem.*, 2005, **70**, 2219-2224.
4. C. Han and J. A. Porco, Jr., *Org. Lett.*, 2007, **9**, 1517-1520.
5. Z.-H. Fu and Y. Ono, *J. Mol. Catal.*, 1994, **91**, 399-405.
6. L. Zhang, Y. Yang, Y. Xue, X. Fu, Y. An and G. Gao, *Catal. Today*, 2010, **158**, 279-285.
7. T. Baba, A. Kobayashi, T. Yamauchi, H. Tanaka, S. Aso, M. Inomata and Y. Kawanami, *Catal. Lett.*, 2002, **82**, 193-197.

8. T. Baba, A. Kobayashi, Y. Kawanami, K. Inazu, A. Ishikawa, T. Echizenn, K. Murai, S. Aso and M. Inomata, *Green Chem.*, 2005, **7**, 159-165.
9. E. Reixach, N. Bonet, F. X. Rius-Ruiz, S. Wershofen and A. Vidal-Ferran, *Ind. Eng. Chem. Res.*, 2010, **49**, 6362-6366.
10. S. Grego, F. Arico and P. Tundo, *Pure Appl. Chem.*, 2012, **84**, 695-705.
11. E. Reixach, R. M. Haak, S. Wershofen and A. Vidal-Ferran, *Ind. Eng. Chem. Res.*, 2012, **51**, 16165-16170.
12. F. Li, H. Xu, W. Xue, Y. Wang and X. Zhao, *Chem. Eng. Sci.*, 2015, **135**, 217-222.
13. G. Wang, D. Ma, X. Jia, X. Cui, X. Zhao and Y. Wang, *Ind. Eng. Chem. Res.*, 2016, **55**, 8011-8017.
14. F. Li, X. Wang, H. Li, S. Wang, W. Xue and Y. Wang, *Catal. Lett.*, 2017, **147**, 1478-1484.
15. X. Zhao, L. Kang, N. Wang, H. An, F. Li and Y. Wang, *Ind. Eng. Chem. Res.*, 2012, **51**, 11335-11340.
16. M. Curini, F. Epifano, F. Maltese and O. Rosati, *Tetrahedron Lett.*, 2002, **43**, 4895-4897.
17. S. Kumar and S. L. Jain, *New J. Chem.*, 2013, **37**, 2935-2938.
18. W. Guo, J. González-Fabra, N. A. G. Bandeira, C. Bo and A. W. Kleij, *Angew. Chem., Int. Ed.*, 2015, **54**, 11686-11690.
19. G. R. Wang, Y. J. Wang and X. Q. Zhao, *Chem. Eng. Technol.*, 2005, **28**, 1511-1517.
20. X. Zhao, Y. Wang, S. Wang, H. Yang and J. Zhang, *Ind. Eng. Chem. Res.*, 2002, **41**, 5139-5144.
21. X. Guo, Z. Qin, W. Fan, G. Wang, R. Zhao, S. Peng and J. Wang, *Catal. Lett.*, 2009, **128**, 405-412.
22. Y. Wang and B. Liu, *Catal. Sci. Technol.*, 2015, **5**, 109-113.
23. F. Li, W. Li, J. Li, W. Xue, Y. Wang and X. Zhao, *Appl. Catal., A*, 2014, **475**, 355-362.
24. S. Biswas, R. Khatun, M. Sengupta and S. M. Islam, *Mol. Catal.*, 2018, **452**, 129-137.
25. F. Li, J. Miao, Y. Wang and X. Zhao, *Ind. Eng. Chem. Res.*, 2006, **45**, 4892-4897.
26. N. Lucas, A. P. Amrute, K. Palraj, G. V. Shanbhag, A. Vinu and S. B. Halligudi, *J. Mol. Catal. A: Chem.*, 2008, **295**, 29-33.
27. F. Li, Y. Wang, W. Xue and X. Zhao, *J. Chem. Technol. Biotechnol.*, 2009, **84**, 48-53.
28. S. Grego, F. Arico and P. Tundo, *Org. Process Res. Dev.*, 2013, **17**, 679-683.
29. S. Kumar and S. L. Jain, *Dalton Trans.*, 2013, **42**, 15214-15218.
30. R. Juarez, P. Concepcion, A. Corma, V. Fornes and H. Garcia, *Angew. Chem., Int. Ed.*, 2010, **49**, 1286-1290.
31. S. Laursen, D. Combata, A. B. Hungria, M. Boronat and A. Corma, *Angew. Chem., Int. Ed.*, 2012, **51**, 4190-4193.
32. N. Stock and S. Biswas, *Chem. Rev.*, 2012, **112**, 933-969.
33. H.-C. Zhou, J. R. Long and O. M. Yaghi, *Chem. Rev.*, 2012, **112**, 673-674.
34. G. Férey, M. Haouas, T. Loiseau and F. Taulelle, *Chem. Mater.*, 2014, **26**, 299-309.
35. R. J. Kuppler, D. J. Timmons, Q.-R. Fang, J.-R. Li, T. A. Makal, M. D. Young, D. Yuan, D. Zhao, W. Zhuang and H.-C. Zhou, *Coord. Chem. Rev.*, 2009, **253**, 3042-3066.
36. P. Garcia-Garcia, J. M. Moreno, U. Diaz, M. Bruix and A. Corma, *Nat. Commun.*, 2016, **7**, 10835.
37. P. Garcia-Garcia, M. Muller and A. Corma, *Chem. Sci.*, 2014, **5**, 2979-3007.
38. S. Rojas-Buzo, P. Garcia-Garcia and A. Corma, *ChemCatChem*, 2017, **9**, 997-1004.
39. J. Liang, Z. Liang, R. Zou and Y. Zhao, *Adv. Mater.*, 2017, **29**, 1701139.
40. L. Zhu, X.-Q. Liu, H.-L. Jiang and L.-B. Sun, *Chem. Rev.*, 2017, **117**, 8129-8176.
41. M. Rimoldi, A. J. Howarth, M. R. DeStefano, L. Lin, S. Goswami, P. Li, J. T. Hupp and O. K. Farha, *ACS Catal.*, 2017, **7**, 997-1014.
42. Y. Liu, R. C. Klet, J. T. Hupp and O. Farha, *Chem. Commun.*, 2016, **52**, 7806-7809.
43. S.-Y. Moon, Y. Liu, J. T. Hupp and O. K. Farha, *Angew. Chem., Int. Ed.*, 2015, **54**, 6795-6799.
44. S. Rojas-Buzo, P. Garcia-Garcia and A. Corma, *ChemSusChem*, 2018, **11**, 432-438.
45. E. Plessers, G. Fu, C. Y. X. Tan, D. E. De Vos and M. B. J. Roeffaers, *Catalysts*, 2016, **6**, 104-111.
46. A. Dhakshinamoorthy, M. Alvaro and H. Garcia, *Appl. Catal., A*, 2010, **378**, 19-25.
47. M. J. Cliffe, W. Wan, X. Zou, P. A. Chater, A. K. Kleppe, M. G. Tucker, H. Wilhelm, N. P. Funnell, F.-X. Coudert and A. L. Goodwin, *Nat. Commun.*, 2014, **5**, 4176.
48. H. Furukawa, F. Gandara, Y.-B. Zhang, J. Jiang, W. L. Queen, M. R. Hudson and O. M. Yaghi, *J. Am. Chem. Soc.*, 2014, **136**, 4369-4381.
49. Z. Hu, Y. Peng, Y. Gao, Y. Qian, S. Ying, D. Yuan, S. Horike, N. Ogiwara, R. Babarao, Y. Wang, N. Yan and D. Zhao, *Chem. Mater.*, 2016, **28**, 2659-2667.
50. Z. Hu, Y. Peng, K. M. Tan and D. Zhao, *CrystEngComm*, 2015, **17**, 7124-7129.
51. J. Jiang, F. Gandara, Y.-B. Zhang, K. Na, O. M. Yaghi and W. G. Klemperer, *J. Am. Chem. Soc.*, 2014, **136**, 12844-12847.
52. F. Li, R. Min, J. Li, L. Gao, W. Xue, Y. Wang and X. Zhao, *Ind. Eng. Chem. Res.*, 2014, **53**, 5406-5412.
53. I. Luz, M. Soukri and M. Lail, *Chem. Mater.*, 2017, **29**, 9628-9638.
54. G. Cirujano Francisco, I. Luz, M. Soukri, C. Van Goethem, F. J. Vankelecom Ivo, M. Lail and E. De Vos Dirk, *Angew. Chem., Int. Ed.*, 2017, **56**, 13302-13306.
55. J. He, X. Duan and C. Li, *Mater. Chem. Phys.*, 2001, **71**, 221-225.
56. R. Juarez, A. Padilla, A. Corma and H. Garcia, *Catal. Commun.*, 2009, **10**, 472-476.
57. B. Francesca, D. Alessandro, B. Silvia, S. Maurizio, T. Pietro and Z. Adriano, *Angew. Chem., Int. Ed.*, 2005, **44**, 4774-4777.